Biomaterials 178 (2018) 728–737

Contents lists available at ScienceDirect

Biomaterials

journal homepage: www.elsevier.com/locate/biomaterials

From neutral to zwitterionic poly(α-amino acid) nonfouling surfaces: Effects of helical conformation and anchoring orientation

Chong Zhang, Jingsong Yuan, Jianhua Lu, Yingqin Hou, Wei Xiong, Hua Lu*

Beijing National Laboratory for Molecular Sciences, Center for Soft Matter Science and Engineering, Key Laboratory of Polymer Chemistry and Physics of Ministry of Education, College of Chemistry and Molecular Engineering, Peking University, Beijing, 100871, People's Republic of China

ARTICLE INFO

Article history:
Received 4 December 2017
Received in revised form
20 January 2018
Accepted 29 January 2018
Available online 3 February 2018

Keywords:
Polypeptides
Poly(amino acid)
Helix
Nonfouling surfaces
Zwitterionic polymer

ABSTRACTS

The development of high-performance nonfouling polymer surfaces for implantable medical devices and therapeutic nanomaterials is of great importance. Elaborating the relationship of polymer structural characteristics and the resulted surface properties can offer useful guidance toward ideal biointerfaces. In this work, we investigate the effects of the helical conformation and anchoring orientation of poly(α-amino acid)s (PαAAs) to produce advanced nonfouling surfaces. By using the neutral poly(γ-(2-(2-(2-methoxyethoxy)ethoxy)ethoxy)esteryl glutamates) (P(EG_3Glu)s) as a model system, the adsorption kinetics are monitored by ex-situ variable angle spectroscopic ellipsometry and in-situ quartz crystal microbalance with dissipation. It is found that the polymers adopting a rigid rod-like α-helical conformation can self-assemble more rapidly to produce denser adlayers, and generate significantly improved nonfouling surfaces compared to those flexible polymer analogues including the widely used antifouling polymer PEG. Moreover, the surface properties can be further enhanced by using the antiparallel orientated helical P(EG_3Glu)s. Most importantly, the insights gained from the P(EG_3Glu) model system are successfully applied to the generation of ultra-low-fouling surfaces using zwitterionic PαAAs brushes, underscoring the generality of the approach. Particularly, the surface based on the antiparallel aligned zwitterionic helical PαAAs exhibits ~98–99% reduction of human serum adsorption relative to the bare gold, and gives almost no adhesion of mouse platelet. Taken together, this work depicts an extremely simple yet highly effective approach to manipulate surface properties for numerous applications in biomaterial interfaces, diagnostics, and biosensors.

1. Introduction

Polymer brushes are covalently attached thin films on surfaces such as gold, titanium dioxide, and silicon [1,2]. The brushes can largely modulate and improve the properties and functions of the coated surfaces including anti-fouling, lubrication, colloidal stabilization, and corrosion protection [3–6]. For example, nonfouling polymer brushes have been proven one of the most useful strategies to prevent nonspecific adsorption of undesirable biomolecules on material surfaces, which, if untreated, would otherwise lead to many adverse events including bacterial infection, rapid blood clearance of nanocarriers, and decreased sensitivity of biosensor [7–9]. Over the past few decades, a variety of synthetic polymers have been explored as nonfouling polymer brushes, including poly(ethylene glycol) (PEG) [10,11], poly(2-oxazoline)s [12,13], zwitterionic polymers [14,15], and polypeptoids [16,17]. Often, the configurational mobility of these polymers is believed to play an important role in blocking protein interaction sites through the so-called steric excluded volume effects [18,19]. In this regard, flexible polymers with large hydrodynamic volumes are often favored in the design of nonfouling materials. However, recent studies have also shown that conformation-constrained architectures such as dendrons [20], loops [21,22], and cycles [23] can generate denser brushes with respect to their linear analogues exhibiting high conformational flexibility. These inspiring advances urge more careful structure-function relationship analysis in order to precisely manipulate the surface properties with different polymer architectures and conformations.

In the present work, we ask the question whether the secondary structures such as the α-helix of synthetic polypeptides, also known as poly(α-amino acid)s (PαAAs), could impact their behaviors on surfaces [24–28]. By simply switching the chirality of the

* Corresponding author.
E-mail address: chemhualu@pku.edu.cn (H. Lu).

https://doi.org/10.1016/j.biomaterials.2018.01.052
0142-9612/

monomeric amino acid of PαAAs, it allows one to facilely tune the conformations with minimum structural perturbance (e.g. the helix-coil transition). In solution, such conformational switches have been shown to cause dramatic property changes including membrane activity [29], gene transfection [30], self-assembled structures [31–33] and antimicrobial efficiency [34]. On surfaces, for example, Li recently demonstrated that cells could adhere and proliferate better on $_{L}$-type poly-γ-benzyl-glutamate grafted surfaces compared with those grafted with $_{D}$-type or $_{DL}$-type analogues [35]. Another appealing feature of studying the helical PαAAs for surface applications is the potential of harnessing the macroscopic dipole moment of the polymers. Specifically, each amino acid of the α-helical PαAA is known to contribute a dipole moment of ~3.5 D derived from the unidirectional orientation of the backbone hydrogen bonding, which can further accumulate into a macroscopic dipole moment from the *N*- to the *C*-terminus of the polymer [36,37]. We expect that this dipole effect could be used to modulate the surface properties by controlling the orientation of PαAAs (parallel or anti-parallel). For example, Higashi and coworkers have shown that helix-helix macrodipole interaction could be used to precisely control the location of a redox moiety in self-assembled monolayers [38,39]. More recently, Cheng and Lin et al. elegantly demonstrated that the helical dipole played an important role in affording ultra-fast polymerization for the synthesis of brush-like polymers [40]. Together, these unique features make PαAAs ideal materials to study the conformation and anchoring orientation effect on nonfouling performance, which has been very rarely investigated before.

2. Materials and methods

2.1. General

Materials Ultrapure water prepared by a Millipore water purification system (Millipore, 18.2 MΩ cm) was used for surface experiments and buffer solutions. Phosphate buffered saline (PBS: 137 mM NaCl, 2.7 mM KCl, 2 mM KH_2PO_4, and 10 mM Na_2HPO_4; pH 7.4 at 25 °C) was freshly prepared, filtered through a 0.22 μm cellulose membrane and degassed by ultrasonication for 10 min before use. Anhydrous *N*,*N*-dimethylformamide (DMF) and hexamethyldisilazane (HMDS) were purchased from Sigma-Aldrich (St. Louis, MO, U.S.A.). Bis(2-dimethylaminoethyl) disulfide dihydrochloride was purchased from TCI, Inc. 2,2-Dimethoxy-2-phenylacetophenone (DMPA), trifluoroacetic acid (TFA), tert-butyl bromoacetate were obtained from Aladdin Reagent Co. Ltd. (Shanghai, China). *S*-trityl-3-mercaptopropionic acid [41], 2-(tritylthio)ethanamine [42], 2-(2-(2-(allyloxy)ethoxy)ethoxy)ethanol [43], γ-(2-(2-(2-Methoxyethoxy)ethoxy)ethoxy)esteryl $_{L}$-glutamate-*N*-carboxyanhydride (($_{L}$-EG$_3$Glu)-NCA), and γ-(2-(2-(2-Methoxyethoxy)ethoxy)ethoxy)esteryl $_{D}$-glutamate-*N*-carboxyanhydride (($_{D}$-EG$_3$Glu)-NCA) [44] were synthesized following procedures described previously. *S*-trityl-3-mercaptopropionicacid anhydride was synthesized in the presence of 1,3-dicyclohexylcarbodiimide (DCC, from Aladdin) as a dehydrating agent [45]. All other chemicals were purchased from commercial sources and used as received unless otherwise specified.

Instrumentation: ^{1}H NMR spectra were recorded using an AVANCE 400 spectrometer (Bruker Biospin, Switzerland). Deuteroxide (D_2O) or deuterated chloroform ($CDCl_3$) was used as the solvent for ^{1}H NMR measurements. Fourier transform infrared spectroscopy (FT-IR) was recorded using a Bruker Tensor 27 FT-IR spectrometer (Bruker, Bremen, Germany) in the range of 400–4000 cm^{-1} at a resolution of 2 cm^{-1} and 64 scans. Tandem gel permeation chromatography (GPC) experiments were performed on a system equipped with an isocratic pump (Model 1100, Agilent Technology, Santa Clara, CA), and an Optilab rEX refractive index detector (Wyatt Technology, Santa Barbara, CA). The temperature of the refractive index detectors was 25 °C. Separations were performed using serially connected size exclusion columns (500, 10^3, 10^4 and 10^5 Å Phenogel columns, 5 μm, 7.8 × 300 mm, Phenomenex, Torrance, CA) at 50 °C using DMF containing 0.1 M LiBr as the mobile phase. The molecular weights of all polymers were determined using the *dn/dc* values calculated from internal calibration system provided by Wyatt Technology. Circular dichroism (CD) spectroscopy was carried out on a Bio–Logic MOS 450 CD spectrometer. The polymer solution was placed in a quartz cell with a light path of 1.0 cm. The mean residue molar ellipticity was calculated by the formula: [θ] in deg·cm^2 dmol^{-1} = (millidegrees × mean residue weight)/(pathlength in millimeters × concentration of polypeptide in mg/mL). The α-helix contents of polypeptides were calculated using the following equation: % α-helix = (-[θ_{222}] + 3000)/39,000 [46]. The topographies of the surfaces were studied by using an atomic force microscope (AFM, Dimension FastScan, Bruker, Germany) in the taping mode. Scanning electron microscopy (SEM) was performed on a Merlin Compact (ZEISS, Germany) field-emission scanning electron microscope at 10 kV.

2.2. Synthesis of monomers and polymers

Synthesis of P(EG$_3$Glu)-*C*-S-Trityl (Scheme S1A)**:** In a glovebox, $_{L}$-EG$_3$Glu-NCA (200 mg, 0.63 mmol, 50 equiv) was dissolved in DMF (4 mL), followed by the addition of initiator 2-(tritylthio)ethanamine (25 μL × 0.5 M, 1.0 equiv). The polymerization solution was stirred for 30 h at room temperature. Upon the completion of polymerization, acetic anhydride (20 equiv) was added to the polymer solution and stirred for another 2 h. The polymer was precipitated in diethyl ether. The obtained polymer was then sonicated for 5 min in diethyl ether and centrifuged to remove the solvent. After repeating this sonication-centrifugation procedure for three times, the product P($_{L}$-EG$_3$Glu)-*C*-S-Trityl was collected and dried under vacuum, yield ~79%. P($_{DL}$-EG$_3$Glu)-*C*-S-Trityl was obtained with ~75% yield by following the same procedure except for using the racemic $_{DL}$-EG$_3$Glu-NCA as the monomer.

Synthesis of P(EG$_3$Glu)-*N*-S-Trityl: In a glovebox, $_{L}$-EG$_3$Glu-NCA (200 mg, 0.63 mmol, 50 equiv) was dissolved in DMF (4 mL), followed by the addition of HMDS (25 μL × 0.5 M, 1.0 equiv) (Scheme S1B). The polymerization solution was stirred at room temperature. Upon the complete consumption of NCAs, *S*-trityl-3-mercaptopropionicacid anhydride (171 mg, 0.25 mmol, 20 equiv) in DMF (1.0 mL) was added to the polymer solution and stirred overnight. The polymer was then precipitated in diethyl ether. The polymer was collected by centrifugation and then sonicated for 5 min in diethyl ether. After repeating this sonication-centrifugation procedure for three times, The product P($_{L}$-EG$_3$Glu)-*N*-S-Trityl was collected and dried under vacuum, yield ~80%. P($_{DL}$-EG$_3$Glu)-*N*-S-Trityl was obtained by the same method except for using the racemic $_{DL}$-EG$_3$Glu-NCA as the monomer, yield ~75%.

Synthesis of zwitterionic thiol *N*,*N*-dimethyl-cysteamine-carboxybetaine (CB-SH): As shown in Scheme S2A, bis(2-dimethylaminoethyl) disulfide dihydrochloride (10.0 g) was neutralized with 3 M NaOH, and the solution was extracted with dichloromethane (200 mL × 3) to afford deprotonated bis(2-dimethylaminoethyl) disulfide after solvent evaporation (6.8 g, yield: 92%). The obtained bis(2-dimethylaminoethyl) disulfide (5.0 g, 24.0 mmol) and *tert*-butyl bromoacetate (14.1 g, 72.1 mmol) were then dissolved in 50 mL acetonitrile and stirred at 60 °C for 24 h. The solution was concentrated, poured into diethyl ether, and stirred for another 12 h to isolate the white precipitate, which was dried under vacuum overnight to get the compound **2** (12.6 g, yield:

88%). For deprotection, compound **2** (6.0 g) was dissolved in DCM (100 mL), to which was slowly added trifluoroacetic acid (15 mL). The solution was stirred overnight at room temperature, concentrated and precipitated into acetone to obtain the compound **3** (2.6 g, yield 80%). To prepare **CB-SH,** compound **3** (2.6 g) was dissolved in MeOH/H_2O (60/30 mL) and to which was added a solution of triphenylphosphine (21.0 g, 80.1 mmol) in DCM (40 mL). The turbid solution was stirred under nitrogen overnight. After the removal of MeOH, the residue was added 50 mL H_2O, and the solution was washed with DCM (50 mL × 3). The pure product **CB-SH** was then obtained as a white powder after lyophilization (2.04 g, yield 78%).

Compound **2**: ^{1}H NMR (400 MHz, $CDCl_3$) δ 4.67 (s, 4 H), 4.45–4.16 (m, 1H), 3.70 (s, 12 H), 3.65–3.52 (m, 4 H), 1.51 (s, 18 H). ^{13}C NMR (400 MHz, $CDCl_3$) δ 163.51, 85.50, 77.40, 77.08, 76.77, 64.47, 62.16, 51.92, 31.64, 28.07.

Compound **3**: ^{1}H NMR (400 MHz, D_2O) δ 4.12 (s, 4 H), 3.90 (m, 4 H), 3.24 (s, 12 H), 3.17–3.00 (m, 4H). ^{13}C NMR (400 MHz, D_2O) δ 166.96, 63.47, 61.73, 52.04, 29.74.

CB-SH: ^{1}H NMR (400 MHz, D_2O) δ 3.95 (s, 2 H), 3.68 (t, 2 H), 3.29–3.07 (s, 6 H), 2.92–2.73 (t, 2 H). ^{13}C NMR (400 MHz, D_2O) δ 167.05, 66.49, 61.81, 51.6, 16.46.

Synthesis of γ-(2-(2-(2-allyloxyethoxy)ethoxy)ethoxy)esteryl $_L$-glutamate-*N*-carboxyanhydride ($_L$-EG$_3$eneGlu-NCA) (Scheme S2B**):** $_L$-glutamic acid (3.0 g, 20.4 mmol) was suspended and stirred in 2-(2-(2-(allyloxy)ethoxy)ethoxy)ethanol (11.4 g, 60 mmol). In an ice bath at 0 °C, sulfuric acid (1.8 mL, 33.7 mmol) was added drop-wise over a period of 10 min. The resulting mixture was stirred at room temperature overnight. Then, the precipitate was isolated by slowly pouring the viscous solution into a mixture of trimethylamine/isopropanol (*v*/*v*: 20/300 mL). After vacuum drying at 50 °C, γ-(2-(2-(2-allyloxyethoxy)ethoxy)ethoxy)esteryl $_L$-glutamate ($_L$-EG$_3$eneGlu) was obtained as pale yellow solid. $_L$-EG$_3$eneGlu was purified by recrystallization in methanol/diethyl ether (*v*/*v*: 20/200) and completely dried before cyclization to get white solid product (3.0 g, yield 46%). The purified $_L$-EG$_3$eneGlu (1.0 g, 3.1 mmol) was dissolved in dry THF (30 mL) under nitrogen and to the solution was added triphosgene (344 mg, 1.16 mmol). The suspension was stirred at 50 °C for 4 h to obtain a clear solution. After the removal of solvent under vacuum, the crude $_L$-EG$_3$eneGlu-NCA was purified via silica column chromatography using ethyl acetate-petroleum ether (*v*/*v*: from 1/4 to 1/1) as the eluent. $_D$-EG$_3$eneGlu-NCA was synthesized by following the same method.

$_L$-EG$_3$eneGlu: ^{1}H NMR (400 MHz, D_2O) δ 5.85 (m, 1H), 5.31–5.11 (m, 2H), 4.25–4.11 (m, 2H), 3.97 (d, 2H), 3.68 (dd, 2H), 3.61 (dd, 9H), 2.55–2.45 (m, 2H), 2.15–1.97 (m, 2H). ^{13}C NMR (400 MHz, D_2O) δ 174.51, 173.77, 133.67, 118.44, 71.74, 69.72–69.40, 68.70, 68.42, 64.08, 53.98, 53.90, 29.79, 25.40. FT-IR (cm^{-1}): 2934 cm^{-1}, 2873 cm^{-1}, 2678 cm^{-1}, 1738 cm^{-1}, 1609 cm^{-1}, 1584 cm^{-1}, 1511 cm^{-1}, 1412 cm^{-1}, 1325 cm^{-1}, 1113 cm^{-1}, 996 cm^{-1}, 923 cm^{-1}.

$_L$-EG$_3$eneGlu-NCA: ^{1}H NMR (400 MHz, $CDCl_3$) δ 7.30 (s, 1H), 5.90 (m, 1H), 5.38–5.15 (m, 2H), 4.52–4.44 (m, 1H), 4.43–4.17 (m, 2H), 4.01 (d, 2H), 3.86–3.48 (m, 10H), 2.53 (m, 2H), 2.42–2.00 (m, 2H). ^{13}C NMR (400 MHz, $CDCl_3$) δ 171.80, 170.28, 151.83, 134.43, 117.59, 72.19, 70.48, 70.24, 69.32, 68.68, 63.51, 57.20, 30.39, 27.05. FT-IR (cm^{-1}): 3265 cm^{-1}, 2919 cm^{-1}, 2871 cm^{-1}, 1855 cm^{-1}, 1788 cm^{-1}, 1735 cm^{-1}, 1614 cm^{-1}, 1450 cm^{-1}, 1352 cm^{-1}, 1113 cm^{-1}, 922 cm^{-1}.

Synthesis of P(EG$_3$eneGlu)-*C*-*S*-Trityl and P(EG$_3$eneGlu)-*N*-*S*-Trityl: P(EG$_3$eneGlu)-*C*-*S*-Trityl and P(EG$_3$eneGlu)-*N*-*S*-Trityl were synthesized by following a similar method used for P(EG$_3$Glu)-*C*-*S*-Trityl and P(EG$_3$-Glu)-*N*-*S*-Trityl synthesis (Scheme S2C and Scheme S2D).

General procedure for the synthesis of zwitterionic polypeptide P(CB-EG$_3$Glu)-*C*-*S*-Trityl via thiol-ene reaction: P(EG$_3$eneGlu)-*C*-*S*-Trityl (20.0 mg, 0.066 mmol "ene"), CB-SH (58.5 mg, 0.33 mmol "thiol") and DMPA (1.8 mg, 0.007 mmol) were dissolved in a DMF/water mixture (2.0/0.5 mL). The vial was purged with nitrogen for 10 min and sealed with a rubber septum. The mixture was irradiation with a 365 nm UV lamp (1.0 W/cm^2) for 6 h, followed by another 6 h irradiation after the addition of 2 mL DI water and 1.8 mg DMPA. The product was purified using a PD-10 column and lyophilized to afford a white solid (yield 70–85%).

Cleavage of the Trityl Protective Group: Taking P($_L$-EG$_3$Glu)-*C*-*S*-Trityl as an example, typically, the precursor polymer (50 mg, 0.004 mmol) was dissolved in anhydrous DCM (2 mL) and trifluoroacetic acid (TFA, 0.5 mL) under nitrogen. After cooling to 0 °C, triethylsilane (TES, 20 μL) was added to the above solution, which was then stirred at room temperature for 6 h. The solution was concentrated and the product was isolated by precipitation in diethyl ether. The obtained polymer was then sonicated for 5 min in diethyl ether and centrifuged to remove the solvent. After repeating the sonication-centrifugation cycle for three times, the polymer P($_L$-EG$_3$Glu)-*C*-SH (L-C) was collected, dried under vacuum and stored in −20 °C freezer in sealed vials before usage, yield ~85%.

2.3. Preparation of monolayers on gold substrates

All gold substrates were cleaned by treating with freshly prepared Piranha solution (H_2SO_4:H_2O_2, 7/3 *v*/*v*) at 60 °C for 15 min, washed with ultrapure water, and blow dried with nitrogen. The polymers at different concentrations (from 1.0×10^{-5} to 5.0 mg/mL) were prepared in PBS buffer (pH 7.4) by a stepwise dilution method. The L-C/L-N solution was prepared by mixing an equal volume of L-C and L-N solution each at half of the final concentration, whereas DL-C/DL-N was made by mixing an equal volume of DL-C and DL-N each at half of the final concentration. The cleaned substrates were then immersed into the polymer solutions and incubated on an oscillator at room temperature for different periods of time (10 min, 0.5, 1, 2, 6, 12 and 24 h). Finally, the coated substrates were rinsed with ultrapure water thoroughly and dried with a stream of nitrogen.

2.4. Characterization of polymer brushes

X-ray photoelectron spectroscopy (XPS): XPS analysis was performed on an X-ray photoelectron spectrometer (Axis Ultra, Kratos Analytical Ltd.) using monochromatic Al Kα (1486.6 eV) as the radiation source.

Static water contact angle (SCA): SCAs of the adlayers were measured at room temperature using a DSA-100 (Kruss, Germany). Water drops (2.0 μL) were deposited on tested surfaces and the values were recorded after 10 s. At least three independent measurements were performed on each sample.

Variable angle spectroscopic ellipsometry (VASE): The thickness of the dried polymer adlayers on the gold surface was measured under ambient conditions by a variable angle spectroscopic ellipsometry (VASE) M2000V (J. A. Woollam, USA) in the spectral range of 370–1000 nm at two incident angles of 70° and 80°. The VASE spectra were then fitted with the multilayer model utilizing CompleteEASE (Version: 4.81) analysis software based on the optical properties of a generalized Cauchy layer model (A = 1.45, B = 0.01, C = 0) [47] to obtain the thickness of the polymer adlayer. The measurements were performed on three independent samples and the thicknesses were reported as mean ± standard deviation (SD).

Real-time monitoring of polymer adsorption by QCM-D: In situ monitoring of the polymer brush formation was recorded on a Q-sense E4 (Q-Sense, Sweden) Quartz crystal microbalance with dissipation (QCM-D). Before the polymer adsorption, a new QCM chip was cleaned by washing with ethanol and water, dried under

N_2, and placed into the flow chamber. After a flat baseline was obtained by pumping PBS for a sufficient period of time, the polymer solution in PBS was injected (50 μL/min, 250 μL). The pump was stopped to allow polymer adsorption for 6 h before the chip was flushed with PBS buffer to remove the unbound or physically bound polymers. The hydrated mass of the adlayer was determined by measuring the frequency shift (Δf). All experiments were performed at 25 °C and the fifth overtone (n = 5) was chosen to calculate the adsorbed mass.

2.5. Evaluation of the nonfouling performance of the polymer brushes

Protein adsorption assay: The QCM chips, with or without polymer coating, were first rinsed with PBS buffer to obtain the baseline. At 25 °C and a flow rate of 50 μL/min, a freshly prepared protein solution (BSA or fibrinogen, 1.0 mg/mL) was flowed through the chips for 15 min, followed by flushing the chip surface with PBS buffer for another 15 min to remove the unbound or loosely bound proteins. The amount of protein adsorbed on surfaces was quantified by measuring the frequency shift (Δf) from the fifth overtone (n = 5). The Sauerbrey model ($\Delta m = C \times \Delta f$, C = 17.7 ng/(cm^2 × Hz)) was used to calculate the adsorbed protein mass (Δm, ng/cm^2) on the gold surfaces. The experiments were repeated at least three times on different chips for each adlayer. The results were reported as mean ± SD.

Cell adhesion experiments: The bare gold and polymer-coated surfaces were sterilized by soaking in 70% ethanol, followed by rinsing with sterilized PBS, and then placed into different wells of a 24-well plate. HeLa-eGFP cells were seeded into each well at a density of 1.0×10^4 cells per well. After incubation at 37 °C for 24 h, each sample was rinsed with 4 mL PBS to remove the unattached cells. The images of cell attachment on samples were recorded using a Nikon A1R confocal laser scanning microscope. Three representative images at different locations were selected, and the fluorescence intensities of the adhered cells were quantified. The results were expressed as normalized fluorescence intensities on the modified surface relative to that on the bare gold surface.

Platelet adhesion experiments: Fresh rat blood was mixed immediately with 3.8 wt% sodium citrate solution in a ratio of 9:1 (v/v) and centrifuged at 1000 rpm for 10 min to obtain the platelet-rich plasma (PRP). The unmodified and modified gold chips were first allowed to equilibrate with PBS buffer (pH 7.4) for 2 h, and then 200 μL PRP was introduced to each sample. After incubation at 37 °C under static conditions for 2 h, the gold surface was rinsed with PBS gently to remove loosely adhered platelets. The adherent platelets were further fixed with 2.5% (v/v) glutaraldehyde overnight, and dehydrated serially using 25%, 50%, 75%, 90%, and 100% ethanol for 20 min in each step. The surfaces were dried with a stream of nitrogen and then coated with gold. The level of platelet adhesion was examined by SEM. The number of adhered platelets on the surface was calculated according to four representative SEM images for each sample. The results were expressed as the number of platelets on the modified surface relative to that on the pristine gold surface.

3. Results and discussion

3.1. P(EG$_3$Glu) synthesis and characterization

Poly(γ-(2-(2-(2-methoxyethoxy)ethoxy)ethoxy)esteryl glutamate) (P(EG$_3$Glu)) was selected as a model system owing to its PEG-like side chain, excellent aqueous solubility, and neutral charge. We prepared four different derivatives of P(EG$_3$Glu) bearing different secondary structures and anchoring functional groups (see experimental section, Fig. 1A and Scheme S1). For clarity purpose, here L-C and L-N denoted the two helical P($_L$-EG$_3$Glu) polymers bearing a thiol group at the *C*- and *N*-terminus, respectively. Similarly, DL-C and DL-N denoted the two unstructured P($_{DL}$-EG$_3$Glu) polymers with the thiol group placed at the *C*- and *N*- terminus, respectively. At a feeding monomer to initiator (M/I) of 50/1, gel permeation chromatography (GPC) and ^{1}H NMR spectroscopy indicated that the resulting four polymers shared similar molecular weights (M_ns) and all had narrow polydispersity indices (*Đ*) smaller than 1.10 (Fig. S1, Fig. S2 and Table S1).

The secondary structures of the four polymers in PBS buffer were characterized by circular dichroism (CD) spectroscopy (Fig. 1B). The CD spectra of both L-C and L-N depicted a typical α-helical conformation evidenced by the two negative minima at 208 and 222 nm. The helical contents of the two polymers were ~92 and 95%, respectively (Table S1). In contrast, both the racemic DL-C and DL-N exhibited disordered conformations as shown by the CD spectra. As expected, the equal molar mixture of L-C and L-N (L-C/L-N) displayed an α-helix conformation with helical contents similar to L-C and L-N, whereas the equal molar mixture of DL-C and DL-N (DL-C/DL-N) showed a disordered conformation (Fig. 1B).

3.2. Adlayer preparation and adsorption kinetics

Next, we tailored the surface properties by using the PαAAs described above, which could form adlayers on gold surfaces via the thiol-Au bonding. Fig. 2A–B showed the dry thickness of different P(EG$_3$Glu) adlayers, measured by ellipsometry, as a function of the incubation time. All samples were found to rapidly reach ~75% of their maximum thicknesses within the first 10 min of incubation and gradually climb to the plateaus at ~12 h. Strikingly, the adlayers composed of the helical P($_L$-EG$_3$Glu)s (L-C and L-N) were both appreciably thicker than the ones composed of the unstructured P($_{DL}$-EG$_3$Glu)s (DL-C and DL-N, Fig. 2A). Considering that the polymers shared almost identical chemical composition, we attributed the thickness difference to their varied secondary structures. It was postulated that the rigid and conformation-constrained α-helix could facilitate denser molecular packing and ensure a greater probability of thiol exposure for enhanced surface anchoring. To examine the orientation effect, we prepared the L-C/L-N and DL-C/DL-N adlayers. We noticed a further improvement in the thickness of the L-C/L-N adlayer when compared to that of L-C (Fig. 2B). Notably, the antiparallel anchored DL-C/DL-N gave almost the same thickness as the DL-C adlayer, suggesting that the aforementioned orientation effect was unique to the helical polymers (Fig. 2B). We hypothesize that the antiparallel anchored L-C/L-N adlayer would cancel the repulsive force derived from the dipole moment, which ultimately resulted in denser polymer grafting on the surface when compared with the parallel aligned L-C or L-N adlayer. Overall, L-C/L-N showed ~41% improvement in the dry thickness than the three adlayers based on the flexible P($_{DL}$-EG$_3$Glu)s (DL-C, DL-N, and DL-C/DL-N). We also studied the adlayer formation as a function of the adsorbate concentration (from 0.0001 to 5.0 mg/mL) for a total incubation time of 12 h (Fig. 2C–D). As expected, the thickness of the polymer adlayers grew gradually with the increased polymer concentration. It was found that at the adsorbate concentration as low as 0.1 mg/mL, all adlayers reached ~90% of their own maximum thicknesses. Importantly, the study reconfirmed our previous finding that the helical polymers could give thicker adlayers than those unstructured polymers (Fig. 2C), and the antiparallel anchoring of the helix could further enhance the polymer adsorption (Fig. 2D).

3.3. Surface analysis

XPS was employed to gain information regarding the surface

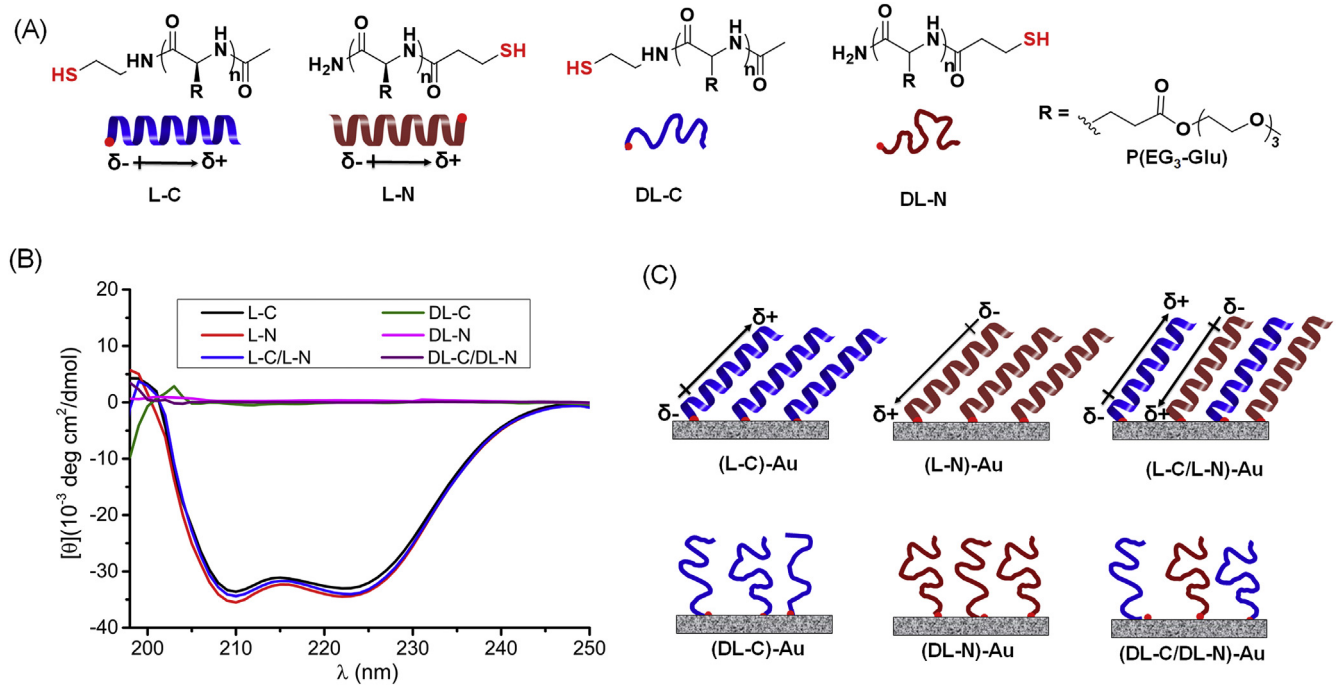

Fig. 1. (A) Chemical structures and secondary conformations of the four P(EG$_3$Glu)s used in the model study (L-C, L-N, DL-C, and DL-N). (B) CD spectra of different P(EG$_3$Glu)s in PBS buffer (pH = 7.4). (C) Cartoon illustration of different PαAA adlayers on Au surfaces.

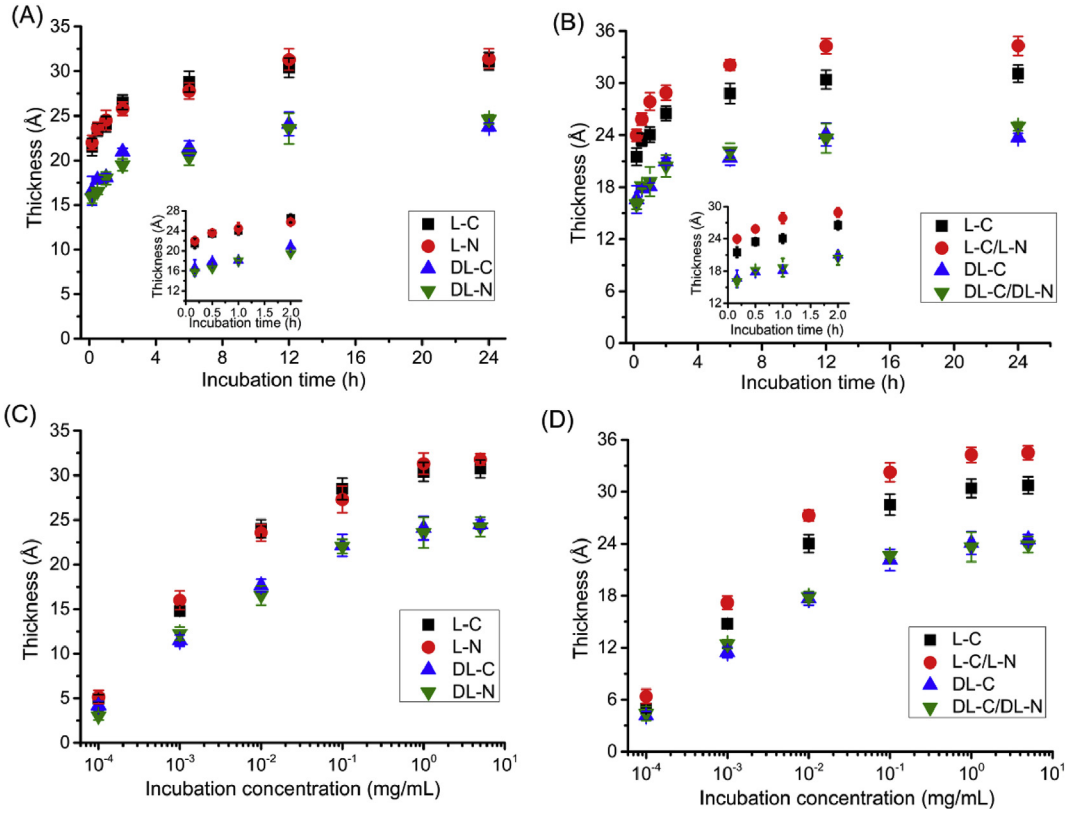

Fig. 2. Ellipsometric thickness of different P(EG$_3$Glu) adlayers in the dry state. (A–B): ellipsometric thickness of P(EG$_3$Glu) adlayers as a function of the adsorption time; the gold surfaces were incubated with different adsorbates at 1.0 mg/mL (Inset: the zoom-in view of the first 2 h); (C–D): ellipsometric thickness of P(EG$_3$Glu) adlayers as a function of the adsorbate concentration; the gold surfaces were incubated with different adsorbate solutions for 12 h.

composition of the PαAA-coated surfaces. Fig. S3A depicted the representative XPS wide scan of the freshly cleaned gold before and after the polymer adsorption. The XPS-derived surface atomic concentrations and molar ratios were listed in Table 1. A substantial

Table 1
XPS-derived surface atomic concentrations and molar ratios of the bare and polymer-modified gold surfaces. Incubation condition: 1.0 mg/mL polymers in PBS for 12 h, 25 °C.

Sample	Atomic concentration (%)					XPS-derived molar ratio				
	Au 4f	C 1s	N 1s	O 1s	S 2p	C/Au[a]	O/Au[a]	O/C[a]	O/N[a]	O–C=O/NH–C=O[b]
Bare gold	66.31	27.42	1.19	5.08	–	0.41	0.08	0.19	4.27	–
L-C	24.04	48.82	4.16	22.07	0.91	2.03	0.92	0.45	5.31	1.00
L-N	23.95	49.16	4.04	22.16	0.69	2.05	0.93	0.45	5.49	0.97
L-C/L-N	19.25	51.03	4.74	23.92	1.06	2.65	1.24	0.47	5.05	0.92
DL-C	28.11	46.67	3.79	20.81	0.62	1.66	0.74	0.45	5.49	1.01
DL-N	27.82	47.51	3.68	20.26	0.73	1.71	0.73	0.43	5.51	0.96
DL-C/DL-N	27.59	47.14	3.82	20.56	0.89	1.71	0.75	0.44	5.38	0.94

[a,b] Calculated from the corresponding surface atomic concentrations and C 1s high resolution spectra, respectively.

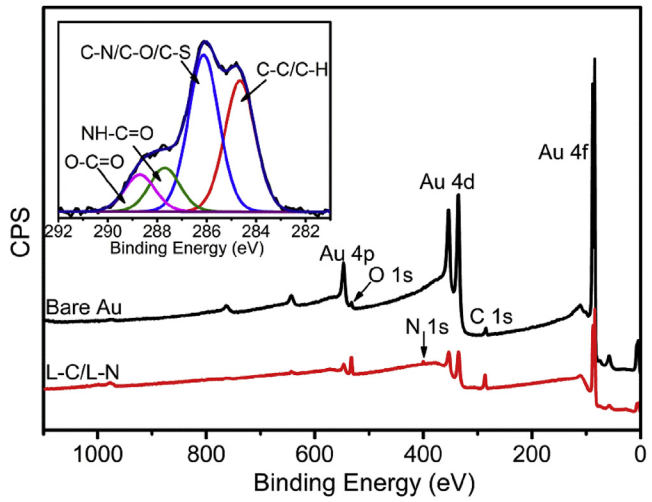

Fig. 3. XPS survey spectra of the bare and representative antiparallel anchored L-C/L-N gold surface. (Inset: narrow scan of the C 1s signal of the L-C/L-N adlayer)

decrease in Au 4f concentration and considerable increases in C 1s, N 1s, O 1s, and S 2p signals were observed following the polymer adsorption. Fitting of the C 1s, N 1s, and O 1s high-resolution scans collectively revealed functional groups corresponding to amide NH–C=O, ester O–C=O, and ether C–O (Fig. 3, Fig. S3B and Fig. S3C). Moreover, the O/C, O/N and O–C=O/NH–C=O ratios of all adlayers were found to match the theoretical values (0.5, 6.0 and 1.0, respectively), an indication of successful PαAA adsorption. Notably, only one thiolate species at ~162.5 eV was detected, suggesting that all the thiol was chemisorbed to the Au surface and thus ruling out the possibility of multilayer adsorption.

The attenuation of the Au 4f signal could also be used as a reference to estimate the adlayer thickness [48]. Among all polymer-coated surfaces, the antiparallel helical L-C/L-N adlayer displayed the lowest Au 4f intensity (~19%), which increased slightly in the helical L-C and L-N adlayers (~24%). The unstructured DL-C, DL-N, and DL-C/DL-N displayed comparable Au 4f intensities between each other (~28%) and were higher than the previous helical polymers. Moreover, L-C/L-N was found to give the highest surface C/Au and O/Au ratios among all tested samples, reconfirming its greatest surface polymer coverage.

The wettability of the surfaces was characterized by SCA (Fig. S4). The SCAs were measured ~85° for the bare gold and ~46° for all the helical P($_{L}$-EG$_3$Glu)-coated surfaces (L-C, L-N, and L-C/L-N). Interestingly, the SCAs of the disordered P($_{DL}$-EG$_3$Glu) adlayers (DL-C, DL-N, and DL-C/DL-N) were ~41°, suggesting a higher degree of wettability of the unstructured polymer adlayers. This was perhaps because the backbone amides in the unstructured polymers remained available for hydration, whereas the same amides were occupied for intramolecular hydrogen bonds in the helical polymers. The morphology of the adlayers was determined by AFM (Fig. S5), which indicated that all the polymers produced uniform structures and exhibited almost similar topography with low average roughness (Ra).

3.4. In-situ QCM-D analysis

Next, we employed quartz crystal microbalance with dissipation (QCM-D) to gain information on the adsorbed mass in the hydrated state and the viscoelastic properties of the forming adlayers in situ. As reflected by the frequency shift (Δf) shown in Fig. 4A, incubation

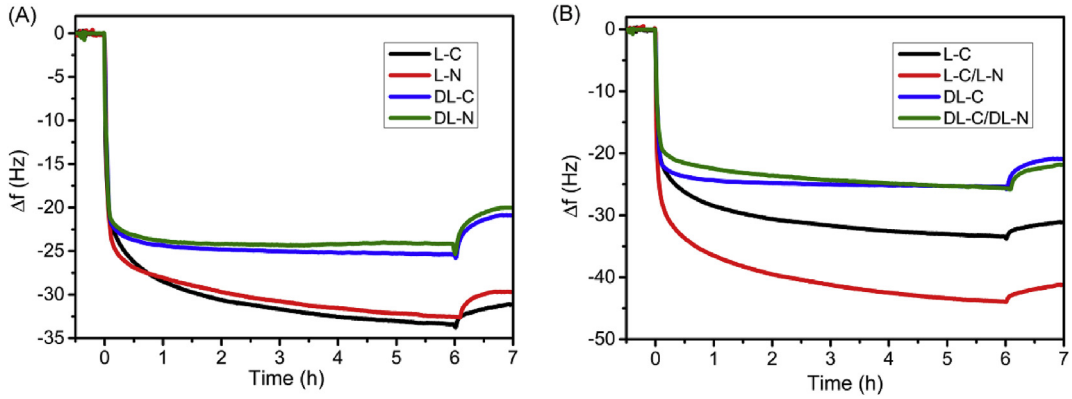

Fig. 4. In-situ QCM-D monitoring of the Δf as a function of the adsorption time for various P(EG$_3$Glu)s.

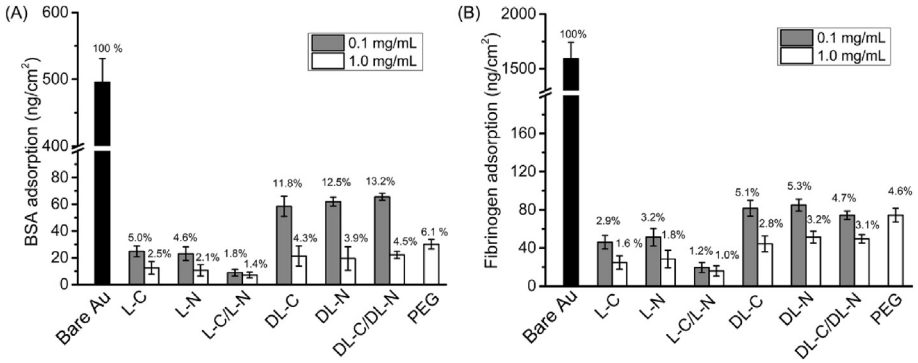

Fig. 5. QCM measurements of BSA (A) and fibrinogen (B) adsorption on P(EG_3Glu)-coated adlayers prepared at 0.1 and 1.0 mg/mL adsorbate concentration for 12 h, respectively. PEG coating was prepared with 1.0 mg/mL adsorbate. The percentage was calculated by normalization of the adsorbed protein on each polymer adlayer to that on the bare gold surface. Results are shown as mean ± SD.

with the helical P($_L$-EG_3Glu)s (L-C or L-N) resulted in faster adsorption kinetics and greater adsorption mass than those unstructured P($_{DL}$-EG_3Glu)s (DL-C or DL-N). Moreover, the equal molar mixed L-C/L-N was found to give the greatest Δf among all the samples tested, which indicated an almost 90% increase of the adsorption mass when compared with DL-C (Fig. 4B). Again, the DL-C/DL-N adlayer showed no difference in final Δf with respect to the DL-C adlayer (Fig. 4B). It is also noteworthy that the L-C/L-N adlayer generated from an equal molar ratio of L-C and L-N displayed the highest amount of polymer adsorption compared with those using polymer mixtures at other molar ratios (Fig. S6A), suggesting the important role of the dipole moment cancellation during the grafting process. To study the viscoelastic properties of the adsorbed layers, the D–f curves (dissipation change (ΔD) against -Δf) of L-C, L-C/L-N, DL-C, DL-C/DL-N adsorption were plotted in Fig. S7. The slopes (∂D/∂f) of L-C and L-C/L-N adsorption were relatively smaller than that of DL-C and DL-C/DL-N, suggesting the helical polymers gave more rigid adlayers than the unstructured polymers [49,50]. Overall, the QCM-D results were in good agreement with the ellipsometry and XPS results discussed above.

3.5. Antifouling properties of P(EG_3Glu)-based adlayers

The antifouling properties of the P(EG_3Glu) adlayers were tested by protein adsorption and cell attachment assays. Fig. 5 showed the adsorbed BSA and fibrinogen masses on bare gold and P(EG_3Glu)-modified surfaces detected by QCM. In general, all surfaces coated with the helical P($_L$-EG_3Glu)s (L-C, L-N, and L-C/L-N) showed considerably less protein binding as compared to those coated with the unstructured P($_{DL}$-EG_3Glu) analogues (DL-C, DL-N, and DL-C/DL-N), with the anti-parallel orientated L-C/L-N gave the best protein resistance. For instance, the L-C/L-N adlayer showed ~3–7 fold less protein adsorption than the DL-C/DL-N adlayer at the same concentration. Most remarkably, the protein resistance of the L-C/L-N adlayer prepared from 0.1 mg/mL adsorbate outperformed all other polymer brushes prepared at 1.0 mg/mL adsorbates. It is also worth mention that the PEG adlayer prepared under a similar condition was comparable to the unstructured DL-C, DL-N, and DL-C/DL-N adlayers, and was considerably less effective than the helical L-C, L-N, and L-C/L-N adlayers. Consistently, our results implied that the L-C/L-N adlayer prepared at an equal molar ratio of L-C and L-N

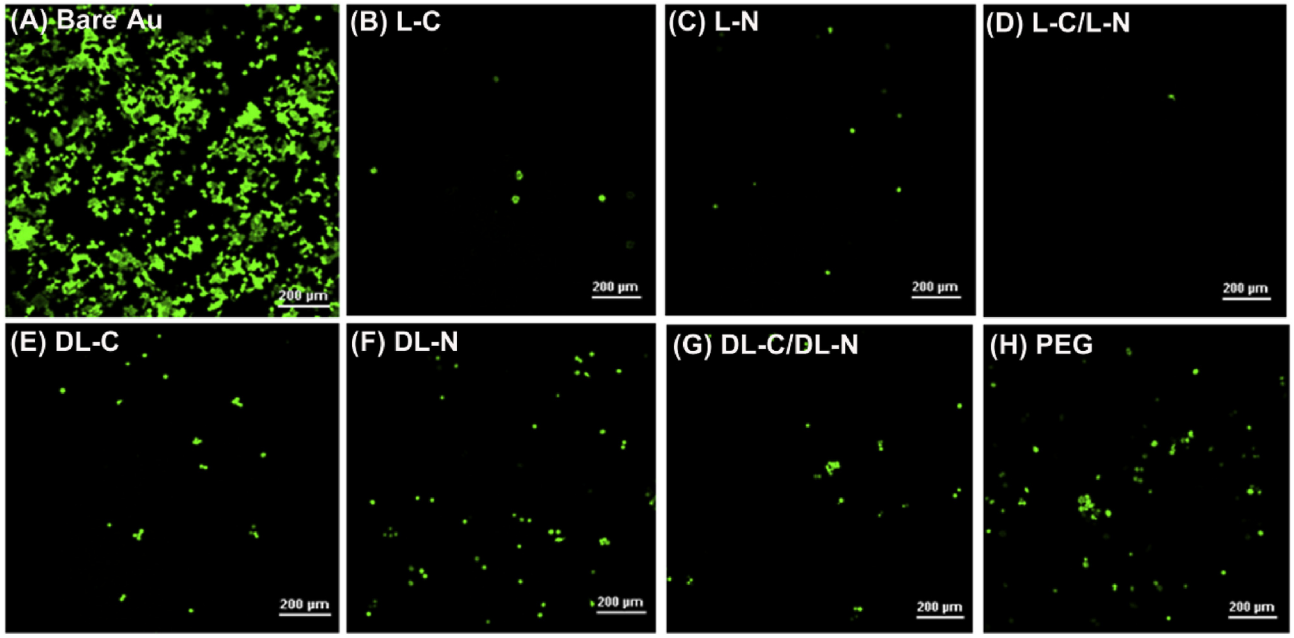

Fig. 6. Fluorescence photographs of eGFP-HeLa cells adsorbed on different P(EG_3Glu)-coated adlayers, scale bar = 200 μm. Adlayer preparation: 12 h incubation with 1.0 mg/mL adsorbate.

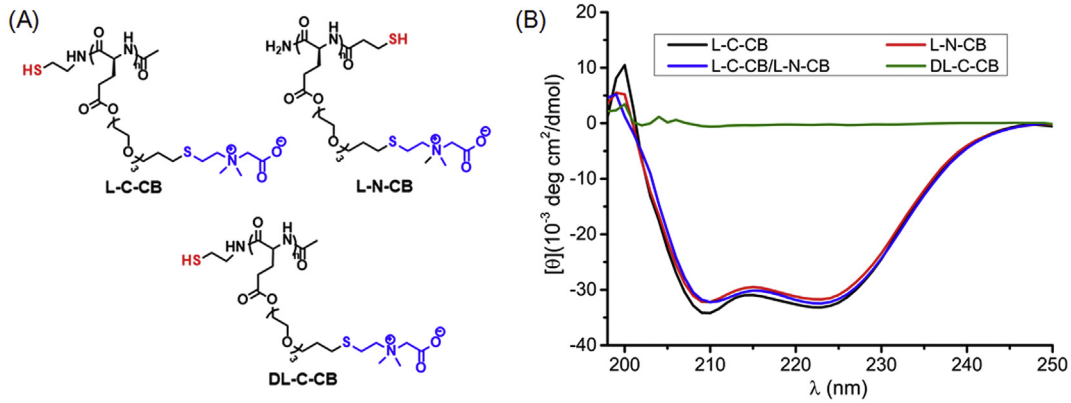

Fig. 7. (A) The structure of the zwitterionic PαAAs: L-C-CB, L-N-CB, and DL-C-CB. (B) CD spectra of different zwitterionic PαAAs in PBS buffer (pH = 7.4).

exhibited the best protein resistance compared to those prepared from the same L-C and L-N polymers but at different molar ratios (Fig. S6B).

Next, we tested the polymer brushes for the prevention of Hela-eGFP cell adhesion. A pattern similar to the protein adsorption was again observed according to the confocal microscopy observation (Fig. 6 and Fig. S8). Briefly, the antiparallel helical L-C/L-N adlayer exhibited the fewest cell attachment, ~3.0% relative to the bare gold surface. In contrast, the parallel helical L-C and the disordered DL-C/DL-N adlayers gave ~9.7 and 13.5% cell contamination with respect to the bare gold.

3.6. Synthesis and antifouling properties of P(CB-EG$_3$Glu)-based adlayers

Zwitterionic polymers have been widely recognized as outstanding nonfouling materials due to their strong electrostatically induced hydration. With the insights obtained from the P(EG$_3$Glu) model system, we reason that the integration of zwitterion and the effects of antiparallel helix could synergistically lead

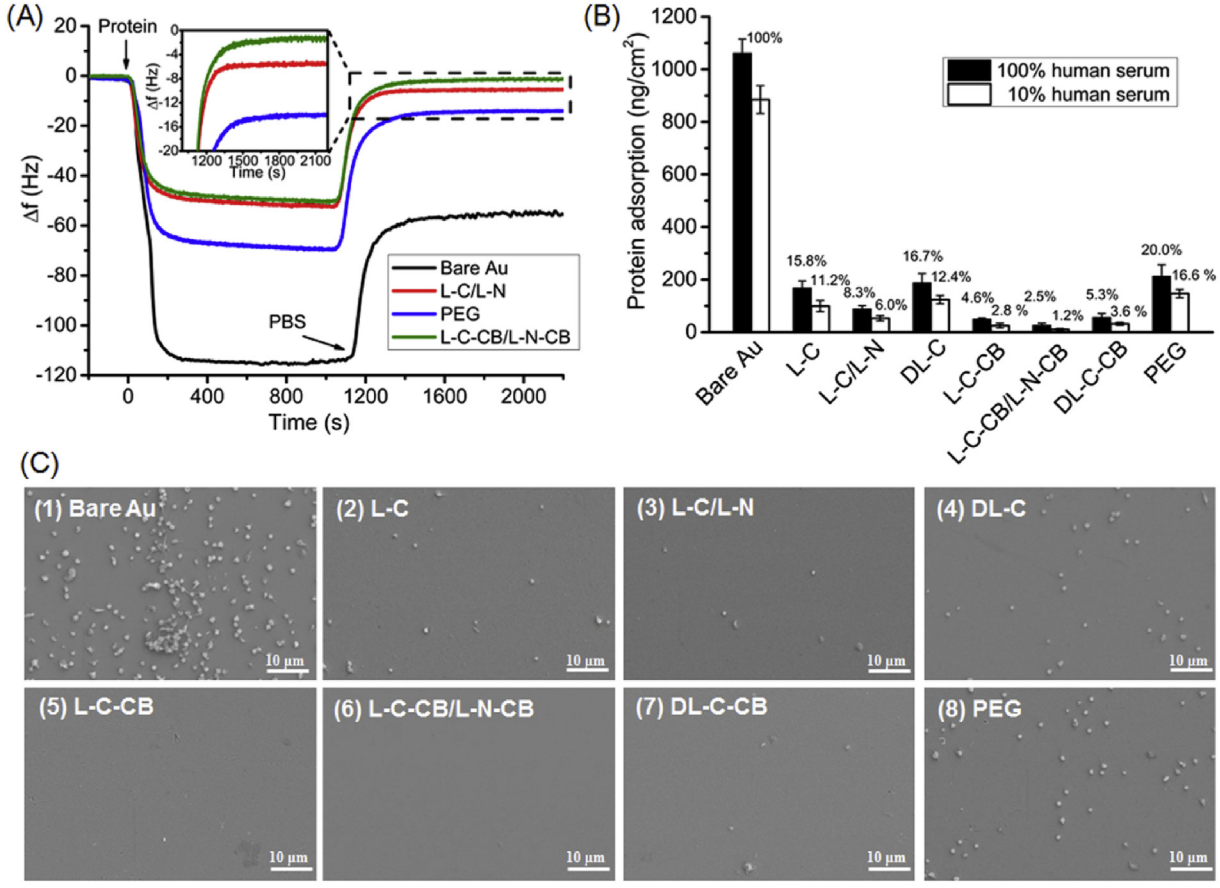

Fig. 8. Nonfouling performance of the zwitterionic helical PαAA adlayers. (A) Representative QCM sensorgrams of the 100% human serum adsorption on various surfaces. (B) The amount of human serum adsorbed on bare gold, the neutral P(EG$_3$Glu) or zwitterionic P(CB-EG$_3$Glu)- coated surfaces. The amount of protein adsorption on each polymer-coated surface was normalized to that on the bare gold surface. (C) Representative SEM images of platelets adhering on pristine (**1**), P(EG$_3$Glu)- (**2**–**4**), P(CB-EG$_3$Glu)- (**5**–**7**) and PEG- (**8**) coated gold surfaces. Magnification: 1500×, scale bar = 10 μm. The adlayers were prepared by incubation with the adsorbate at 1.0 mg/mL for 12 h.

to surfaces with ultra-low fouling. For this, we designed and synthesized two zwitterionic helical PαAAs for the first time (Fig. 7A and Scheme S2). Similar to the neutral P(EG_3Glu) system, the zwitterionic P($_L$-CB-EG_3Glu) bear the *C*- and *N*- terminal thiol was denoted as L-C-CB and L-N-CB, respectively (Fig. S9-S14). Accordingly, a racemic P($_{DL}$-CB-EG_3Glu) with a *C*-terminal thiol was also prepared and denoted as DL-C-CB. The zwitterionic PαAAs shared a similar degree of polymerization ~50 (Table. S2). CD spectra depicted a random coil structure for DL-C-CB and ~90% helicity for L-C-CB, L-N-CB, and the mixed L-C-CB/L-N-CB (Fig. 7B). The P(CB-EG_3Glu) polymers were coated on gold surfaces via the aforementioned protocol and the SCAs of all surfaces were measured to be ~30° (Fig. S15A), which were appreciably smaller than those of P(EG_3Glu) adlayers.

To interrogate the antifouling performance, we first tested the single protein adsorption of the L-C-CB, DL-C-CB, and L-C-CB/L-N-CB adlayers by QCM, and compared to those in P(EG_3Glu)-based L-C/L-N and PEG adlayers. Strikingly, all zwitterionic adlayers exhibited almost no BSA and fibrinogen adsorption (below the lower detection limit of QCM), which outperformed both the L-C/L-N and PEG adlayers (Fig. S15B). Encouraged by this result, we challenged the polymer-coated surfaces with 10% or 100% human serum containing various highly adhesive proteins (Fig. 8A–B) [51]. As the PEG adlayer reduced only ~80–84% serum adsorption relative to the bare gold, the P(EG_3Glu)-based DL-C, L-C, and L-C/L-N adlayers showed a 83–88%, 84–89%, and 92–94% reduction in adsorbed proteins, respectively. To our excitement, the P(CB-EG_3Glu)-based DL-C-CB, L-C-CB, and L-C-CB/L-N-CB adlayers reduced 94–95%, 95–97%, and 98–99% protein adsorption, respectively. Thus, the antiparallel orientated zwitterionic helical L-C-CB/L-N-CB adlayer appeared to be the most effective antifouling surface.

Next, we tested by SEM the ability of the polymer brushes in preventing mouse platelet adhesion, which was a major indicator of hemocompatibility [52]. It was found that many platelets readily adhered on the bare gold surface and formed large aggregates with pseudopodium, suggesting a potential risk of blood coagulation (Fig. 8C). In contrast, the number of adhered platelets decreased substantially for all polymer-coated surfaces. Notably, PEG-coated surface showed a higher platelet adhesion level (20.8%, Fig. 8C and Fig. S16) than the neutral P(EG_3Glu)-based adlayers DL-C, L-C, and L-C/L-N (14.7%, 8.7%, 3.2%, respectively). Consistently, much fewer platelets were detected on the zwitterionic P(CB-EG_3Glu)-based DL-C-CB and L-C-CB adlayers (< 1.0%), with the antiparallel zwitterionic helical L-C-CB/L-N-CB brush gave no platelet adhesion.

4. Conclusions

In summary, we systematically investigated the conformation and anchoring orientation effects of various PαAAs with regard to their adsorption kinetics, surface composition, hydration, morphology, and antifouling properties. Our results indicated that PαAAs with the rigid α-helical structures self-assembled more rapidly, produced denser adlayers, and generated superior antifouling surfaces than those with an unstructured conformation. Furthermore, we found that the surface properties could be further enhanced by the antiparallel anchoring of the helical but not the disordered PαAAs. Because the helical PαAA adlayers appeared to show less hydration than their disordered counterparts, the enhanced antifouling properties of the formers were presumably attributed to the stiffer structural characters and more compact surface packing. More importantly, the conformation and orientation effects demonstrated in the neutral P(EG_3Glu) systems were successfully applied to the design and synthesis of a zwitterionic P(CB-EG_3Glu) system with ultra-low-fouling capacity. This result strongly supported the generality and broad scope of our method. Taken together, this work depicted an extremely simple yet highly effective approach for surface property manipulation, and provided insights useful for numerous applications in biomaterial interfaces, diagnostics, and biosensors.

Conflicts of interest

The authors declare no competing financial interests.

Acknowledgments

This work was financially supported by National Key Research and Development Program of China (2016YFA0201400). We thank the grants from National Natural Science Foundation of China (21722401, 21474004, and 21434008). H. L. thanks the startup funding from Youth Thousand-Talents Program of China. We thank Pro. Haifeng Yu and Dr. Wei Wei for generously sharing the VASE and QCM-D instruments, and also Xiaodi Da for SEM test.

Appendix A. Supplementary data

Supplementary data related to this article can be found at https://doi.org/10.1016/j.biomaterials.2018.01.052.

References

[1] J.O. Zoppe, N.C. Ataman, P. Mocny, J. Wang, J. Moraes, H.A. Klok, Surface-initiated controlled radical polymerization: state-of-the-art, opportunities, and challenges in surface and interface engineering with polymer brushes, Chem. Rev. 117 (2017) 1105–1318.
[2] W.L. Chen, R. Cordero, H. Tran, C.K. Ober, 50th anniversary perspective: polymer brushes: novel surfaces for future materials, Macromolecules 50 (2017) 4089–4113.
[3] I. Banerjee, R.C. Pangule, R.S. Kane, Antifouling coatings: recent developments in the design of surfaces that prevent fouling by proteins, bacteria, and marine organisms, Adv. Mater. 23 (2011) 690–718.
[4] X. Banquy, J. Burdynska, D.W. Lee, K. Matyjaszewski, J. Israelachvili, Bio-inspired bottle-brush polymer exhibits low friction and Amontons-like behavior, J. Am. Chem. Soc. 136 (2014) 6199–6202.
[5] A.B. Lowe, B.S. Sumerlin, M.S. Donovan, C.L. McCormick, Facile preparation of transition metal nanoparticles stabilized by well-defined (co)polymers synthesized via aqueous reversible addition-fragmentation chain transfer polymerization, J. Am. Chem. Soc. 124 (2002) 11562–11563.
[6] W.J. Yang, K.G. Neoh, E.T. Kang, S.L. Teo, D. Rittschof, Polymer brush coatings for combating marine biofouling, Prog. Polym. Sci. 39 (2014) 1017–1042.
[7] C. Blaszykowski, S. Sheikh, M. Thompson, Surface chemistry to minimize fouling from blood-based fluids, Chem. Soc. Rev. 41 (2012) 5599–5612.
[8] X. Ding, C. Yang, T.P. Lim, L.Y. Hsu, A.C. Engler, J.L. Hedrick, Y.Y. Yang, Antibacterial and antifouling catheter coatings using surface grafted PEG-b-cationic polycarbonate diblock copolymers, Biomaterials 33 (2012) 6593–6603.
[9] Q. Yu, Y. Zhang, H. Wang, J. Brash, H. Chen, Anti-fouling bioactive surfaces, Acta. Biomater. 7 (2011) 1550–1557.
[10] J.M. Harris, S. Zalipsky, Poly(ethylene Glycol): Chemistry and Biological Applications, vol. 680, American Chemical Society, Washington, DC, 1997.
[11] S.J. Sofia, V. Premnath, E.W. Merrill, Poly (ethylene oxide) grafted to silicon surfaces: grafting density and protein adsorption, Macromolecules 31 (1998) 5059–5070.
[12] R. Konradi, B. Pidhatika, A. Mühlebach, M. Textor, Poly-2-methyl-2-oxazoline: a peptide-like polymer for protein-repellent surfaces, Langmuir 24 (2008) 613–616.
[13] C. Zhang, S. Liu, L. Tan, H. Zhu, Y. Wang, Star-shaped poly (2-methyl-2-oxazoline)-based films: rapid preparation and effects of polymer architecture on antifouling properties, J. Mater. Chem. B 3 (2015) 5615–5628.
[14] S. Jiang, Z. Cao, Ultralow-fouling, functionalizable, and hydrolyzable zwitterionic materials and their derivatives for biological applications, Adv. Mater. 22 (2010) 920–932.
[15] Z. Zhang, T. Chao, S. Chen, S. Jiang, Superlow fouling sulfobetaine and carboxybetaine polymers on glass slides, Langmuir 22 (2006) 10072–10077.
[16] H.O. Ham, S.H. Park, J.W. Kurutz, I.G. Szleifer, P.B. Messersmith, Antifouling glycocalyx-mimetic peptoids, J. Am. Chem. Soc. 135 (2013) 13015–13022.
[17] S. Xuan, S. Gupta, X. Li, M. Bleuel, G.J. Schneider, D. Zhang, Synthesis and characterization of well-defined pegylated polypeptoids as protein-resistant polymers, Biomacromolecules 18 (2017) 951–964.
[18] B.K.D. Ngo, M.A. Grunlan, Protein resistant polymeric biomaterials, ACS Macro

Lett. 6 (2017) 992–1000.
[19] S.I. Jeon, J.H. Lee, J.D. Andrade, P.G. De Gennes, Protein-surface interactions in the presence of polyethylene oxide: I. Simplified theory, J. Colloid Interface Sci. 142 (1991) 149–158.
[20] T. Gillich, E.M. Benetti, E. Rakhmatullina, R. Konradi, W. Li, A. Zhang, A.D. Schluter, M. Textor, Self-assembly of focal point oligo-catechol ethylene glycol dendrons on titanium oxide surfaces: adsorption kinetics, surface characterization, and nonfouling properties, J. Am. Chem. Soc. 133 (2011) 10940–10950.
[21] T. Kang, X. Banquy, J. Heo, C. Lim, N.A. Lynd, P. Lundberg, D.X. Oh, H.K. Lee, Y.K. Hong, D.S. Hwang, J.H. Waite, J.N. Israelachvili, C.J. Hawker, Mussel-inspired anchoring of polymer loops that provide superior surface lubrication and antifouling properties, ACS Nano 10 (2016) 930–937.
[22] L. Li, B. Yan, L. Zhang, Y. Tian, H. Zeng, Mussel-inspired antifouling coatings bearing polymer loops, Chem. Commun. 51 (2015) 15780–15783.
[23] G. Morgese, L. Trachsel, M. Romio, M. Divandari, S.N. Rama-krishna, E.M. Benetti, Topological polymer chemistry enters surface science: linear versus cyclic polymer brushes, Angew. Chem. Int. Ed. 55 (2016) 15583–15588.
[24] J. Wang, M.I. Gibson, R. Barbey, S.J. Xiao, H.A. Klok, Nonfouling polypeptide brushes via surface-initiated polymerization of N^{ε}-oligo(ethylene glycol)succinate-$_{L}$-lysine N-carboxyanhydride, Macromol. Rapid Commun. 30 (2009) 845–850.
[25] T. Borase, A. Heise, Hybrid nanomaterials by surface grafting of synthetic polypeptides using N-carboxyanhydride (NCA) polymerization, Adv. Mater. 28 (2016) 5725–5731.
[26] Y. Shen, Z. Li, H.A. Klok, Polypeptide brushes grown via surface-initiated ring-opening polymerization of α-amino acid N-carboxyanhydrides, Chin. J. Polym. Sci. 33 (2015) 931–946.
[27] S.H. Wibowo, A. Sulistio, E.H.H. Wong, A. Blencowe, G.G. Qiao, Polypeptide films via N-carboxyanhydride ring-opening polymerization (NCA-ROP): past, present and future, Chem. Commum 50 (2014) 4971–4988.
[28] Y. Ren, R. Baumgartner, H. Fu, P. van der Schoot, J. Cheng, L. Yin, Revisiting the helical cooperativity of synthetic polypeptides in solution, Biomacromolecules 18 (2017) 2324–2332.
[29] M.D. Wyrsta, A.L. Cogen, T.J. Deming, A parallel synthetic approach for the analysis of membrane interactive copolypeptides, J. Am. Chem. Soc. 123 (2001) 12919–12920.
[30] L. Yin, H. Tang, K.H. Kim, N. Zheng, Z. Song, N.P. Gabrielson, J. Cheng, Light-responsive helical polypeptides capable of reducing toxicity and unpacking DNA: Toward nonviral gene delivery, Angew. Chem. Int. Ed. 52 (2013) 9182–9186.
[31] K.S. Krannig, H. Schlaad, pH-responsive bioactive glycopolypeptides with enhanced helicity and solubility in aqueous solution, J. Am. Chem. Soc. 134 (2012) 18542–18545.
[32] E.P. Holowka, D.J. Pochan, T.J. Deming, Charged polypeptide vesicles with controllable diameter, J. Am. Chem. Soc. 127 (2005) 12423–12428.
[33] J. Rodríguez-Hernández, S. Lecommandoux, Reversible inside– out micellization of ph-responsive and water-soluble vesicles based on polypeptide diblock copolymers, J. Am. Chem. Soc. 127 (2005) 2026–2027.
[34] M. Xiong, Z. Han, Z. Song, J. Yu, H. Ying, L. Yin, J. Cheng, Bacteria-assisted activation of antimicrobial polypeptides by a random-coil to helix transition, Angew. Chem. Int. Ed. 56 (2017) 10826–10829.
[35] Y. Ma, Y. Shen, Z. Li, Different cell behaviors induced by stereochemistry on polypeptide brush grafted surfaces, Mater. Chem. Front 1 (2017) 846–851.
[36] A. Wada, The alpha-helix as an electric macro-dipole, Adv. Biophys. 9 (1976) 1–63.
[37] E. Galoppini, M.A. Fox, Effect of the electric field generated by the helix dipole on photoinduced intramolecular electron transfer in dichromophoric α-helical peptides, J. Am. Chem. Soc. 118 (1996) 2299–2300.
[38] M. Niwa, M. Morikawa, N. Higashi, Controllable orientation of helical poly ($_{L}$-glutamic acid) rods through macrodipole interaction on gold surfaces and vectorial electron transfer, Angew. Chem. Int. Ed. 112 (2000) 990–993.
[39] M. Niwa, M. Morikawa, N. Higashi, Discrimination between N-and C-termini of polypeptides by a two-dimensional array of helical poly ($_{L}$-glutamic acid) rods on gold surfaces, Langmuir 15 (1999) 5088–5092.
[40] R. Baumgartner, H. Fu, Z. Song, Y. Lin, J. Cheng, Cooperative polymerization of α-helices induced by macromolecular architecture, Nat. Chem. 9 (2017) 614–622.
[41] J. Bartels, P. Lu, K. Maurer, A.V. Walker, K.D. Moeller, Site-Selectively functionalizing microelectrode arrays: the use of Cu (I)-catalysts, Langmuir 27 (2011) 11199–11205.
[42] P.K. Hashim, K. Okuro, S. Sasaki, Y. Hoashi, T. Aida, Reductively cleavable nanocaplets for sirna delivery by template-assisted oxidative polymerization, J. Am. Chem. Soc. 137 (2015) 15608–15611.
[43] A.V. Chuchuryukin, P.A. Chase, H.P. Dijkstra, B. Suijkerbuijk, A.M. Mills, A.L. Spek, G.P.M. van Klink, G. van Koten, General approach for template-directed synthesis of macroheterocycles by ring-closing metathesis (RCM), Adv. Synth. Catal. 347 (2005) 447–462.
[44] C. Chen, Z. Wang, Z. Li, Thermoresponsive polypeptides from pegylated poly-$_{L}$-glutamates, Biomacromolecules 12 (2011) 2859–2863.
[45] R. Liu, X. Chen, S.H. Gellman, K.S. Masters, Nylon-3 polymers that enable selective culture of endothelial cells, J. Am. Chem. Soc. 135 (2013) 16296–16299.
[46] J.A. Morrow, M.L. Segall, S. Lund-Katz, M.C. Phillips, M. Knapp, B. Rupp, K.H. Weisgraber, Differences in stability among the human apolipoprotein E isoforms determined by the amino-terminal domain, Biochemistry 39 (2000) 11657–11666.
[47] J.N. Hilfiker, R.A. Synowicki, Spectroscopic ellipsometry for polymer thin films, Solid State Technol. 41 (1998) 101–110.
[48] D. Briggs, Surface Analysis of Polymers by XPS and Static SIMS, Cambridge University Press, Cambridge, 1998.
[49] G. Liu, G. Zhang, QCM-D Studies on Polymer Behavior at Interfaces, Springer Heidelberg, New York, 2013.
[50] F. Höök, M. Rodahl, B. Kasemo, P. Brzezinski, Structural changes in hemoglobin during adsorption to solid surfaces: effects of pH, ionic strength, and ligand binding, Proc. Natl. Acad. Sci. U. S. A. 95 (1998) 12271–12276.
[51] G. Gunkel, W.T.S. Huck, Cooperative adsorption of lipoprotein phospholipids, triglycerides, and cholesteryl esters are a key factor in nonspecific adsorption from blood plasma to antifouling polymer surfaces, J. Am. Chem. Soc. 135 (2013) 7047–7052.
[52] N. Huang, P. Yang, Y.X. Leng, J.Y. Chen, H. Sun, J. Wang, G.J. Wang, P.D. Ding, T.F. Xi, Y. Leng, Hemocompatibility of titanium oxide films, Biomaterials 24 (2003) 2177–2187.